PAPER • OPEN ACCESS

Annealing temperature induced improved crystallinity of YSZ thin film

View the article online for updates and enhancements.
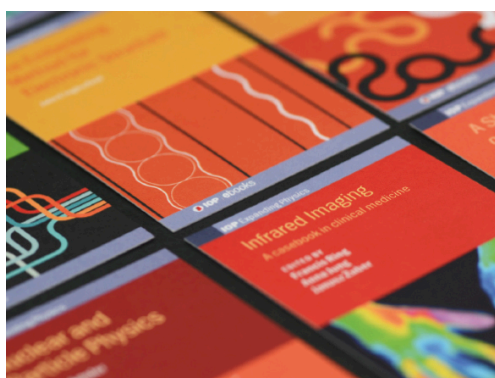
IOP ebooks™

Bringing together innovative digital publishing with leading authors from the global scientific community.

Start exploring the collection–download the first chapter of every title for free.

Materials Research Express

PAPER

Annealing temperature induced improved crystallinity of YSZ thin film

N A Rusli[1] , R Muhammad[1], S K Ghoshal[1], H Nur[2] and N Nayan[3]

1 Department of Physics, Faculty of Science, Universiti Teknologi Malaysia UTM, 81310, Skudai, Johor Bahru, Malaysia
2 Centre for Sustainable Nanomaterials, Ibnu Sina Institute for Scientific and Industrial Research Universiti Teknologi Malaysia UTM, 81310, Skudai Johor Bahru, Malaysia
3 Microelectronics and Nanotechnology—Shamsuddin Centre of Excellence, Universiti Tun Hussein Onn Malaysia, 86400 UTHM Batu Pahat, Johor, Malaysia

E-mail: hamizah_rusli@yahoo.com

Abstract

Six YSZ thin films (YSZTFs) were prepared at varied annealing temperature (380 °C to 600 °C) by radio frequency magnetron sputtering method. Glancing angle x-ray diffraction (GAXRD) pattern revealed the polycrystalline nature of all films with crystallite size in the range of 9 to 15 nm. Sample annealed at 400 °C displayed the lowest microstrain (0.262) and crystallinity (60%). FESEM images disclosed dense, homogeneous and crack free growth of annealed samples compared to as-deposited one. EDX spectra detected the right elemental compositions of films. AFM images showed growth evolution of YSZ grains with size range between 0.2 to 5 nm and improved films' surface roughness. HRTEM measurement of the studied YSZTFs exhibited lattice orientation and atomic structure of nucleated YSZ nanocrystallites. Furthermore, film annealed at 500 °C divulged less oriented structure because of dislocation.

1. Introduction

Conventional electrochemical device called solid oxide fuel cells (SOFCs) utilize fuel and air to produce electricity at high temperature range (800 to 1000 °C) [1–3]. Because of such high operating temperature the electrode, electrolyte, and interconnect covering structure are subjected to physical and chemical stress, leading to deterioration and eventual failure [4, 5]. To overcome such limitations, high resistance thin film electrolytes for SOFC to be operated at low temperature region (down to 300 °C–500 °C) have beeen continually demanded. The solid oxide (called electrolyte) materials being a superionic or fast ion conductors generally consist of highly dense structure to prevent the direct mixing of fuel gas (hydrogen) and oxidizing gas (oxygen) [6]. Dedicated research efforts on solid oxide yttrium stabilized zirconia (YSZ) thin films (TFs) mostly focused on their nanocrystalline structure, formation of phases, control of thickness and conductivity [7–9]. YSZ exists in tetragonal and cubic crystalline phases. Usually, tetragonal structure is not used due to low phase stability. Meanwhile, cubic phase owing to its high crystallinity is very useful as ionic conductors in SOFCs [10, 11]. The ionic conductivity performance of the deposited YSZTFs has been shown to depend on the types of phases' formed, surface microstructure and film thickness.

Like other traditional solid electrolytes, YSZ offer numerous advantages such as phase stability over varied temperature, excellent mechanical properties [12], good compatibility and adaptability to diverse types of electrode-electrolyte based on ceria [13], lanthanum strontium (LS), platinum (Pt), nickel oxide (NiO) [14]. On top, YSZ also acts as bilayer structure with gas tightness. Despite several benefits offered by YSZ electrolyte its applicability is mainly limited due to (i) great sensitivity to deactivation of the ionic conductor under low operating temperature, and (ii) impossibility of low temperature synthesis because of high melting point [15]. These drawbacks allow YSZ electrolyte to be selectively applied for the synthesis of specialty physic [16–19]. In this regard, RF magnetron sputtering became a successful technique because of its ability to deposit high melting

point oxides at low substrate temperatures. Nevertheless, due to very low deposition rate of RF magnetron sputtering method it is difficult to produce fully dense thin films. To improve the RF magnetron sputtered electrolyte characteristic (improve dense structure), Sochugor *et al* [20] demonstrated some strategies wherein the YSZTFs were annealed in the air at 1150 °C for 2 h after the deposition. So far, such YSZTFs have been grown at high annealing temperature (from 600 to 1400 °C) to characterize thoroughly their suructure and morphology [21, 22]. According literature reports, not many efforts have been provided yet to synthesize YSZTFs at low annealing temperature (from 300 to 600 °C).

It known that the films' quality and level of contamination obtained by RF magnetron sputtering method are significant for SOFC working. Actually, one needs film thickness less than 200 nm with dense microstructure. In this sense, the term thin film can be defined as unique material attribute that results from the atomic growth mechanism. The fragile thin film that required to adhere well to the substrate creating well-designed nanostructure with 2 or 3 dimensions is difficult to achieve in bulk materials [23, 24]. The deposition and control of substrate temperature inside a sputtering system are critical for the growth of YSZTFs. When YSZ target is bombarded it responds strongly to the presence of the large lattice mismatch between substrate and thin film materials. If the inter-diffusion adhesion differs, the TFs are subjected to stress/strain effect, grain growth, microstructure evolution and phase transformation thereby influencing the bonding between the film and the substrate [16, 25–28]. Despite many attempts to determine a correlation between the structure and the growth evolution of RF magnetron sputtered YSZTFs, a clear understanding on the effects of annealing temperature (380 °C–600 °C) on deposited films remains deficient. In order to develop high performance electrolyte, it is essential to achieve an in-depth knowledge on the relationship between structural evolution, morphology, physicochemical and ionic conductivity of grown films.

Driven by this idea, this paper evaluates the annealing temperature induced microstructure evolution and improved crystallinity of YSZTFs deposited by RF magnetron sputtering technique. Prepared samples were characterized by diverse analytical tools. Results were analyzed, discussed, interpreted and compared.

2. Materials and methods

Proposed YSZTFs were deposited on glass (SiO_2) substrate using integrated (SNTEK DC and RF) magnetron sputtering technique (model PSP5004 equipped with a high vacuum system) where high purity (99.99%) YSZ target was utilized. First, glass substrates (each of dimension 2 cm × 1 cm) were cleaned successively in an ultrasonic bath using acetone, ethanol and distilled water before being dried in a oven at 120 °C. Then, the sputtering chamber was evacuated to a pressure of 5×10^{-6} Pa via the combination of rotary and turbo-molecular pump. Next, argon (Ar) gas (99.99% pure) was injected into the chamber until the pressure reached to 5 mTorr. Thereafter, the target was cleaned through pre-sputtering (with 50 W RF power) process for 15 min and subject to Ar as working gas at a flow ratio of 100 sccm. For the deposition of all films the separation between the target and the substrate was maintained at 15 cm, wherein the substrate was heated at 300 °C under fixed RF power (100 W).

Crystalline phases of as-prepared YSZTFs were identified via glancing angle x-ray diffractometer (GAXRD, Roguku) equipped with a diffracted beam graphite monochromator. It used Cu-Kα1 radiation of wavelength (λ) 1.5406 Å with angular scanning (2θ) range of 20 to 90° at a scanning rate of 5° per min. The cell parameters of all samples were analyzed at the glancing angle of 1.5°. The microstructure, surface morphology, thickness and elemental traces of studied YSZTFs were determined by field emission scanning electron microscopy (FE-SEM-EDX, Carl Zeiss-Crossbeam 340 model operated at 2 kV). All specimens were pre-sputter by platinum to reduce charging effect emerges due to nonconductive nature of samples. The grain size, topography and surface roughness were examined using atomic force microscopy (NanoNavi AFM interfaced with SPIWin software). High resolution transmission electron microscopy (HRTEM, JEM-2100) was used to image any change in the crystallographic orientation (lattice parameter) of the nanocrystalline grains due to lattice dislocation. Selected angle electron diffraction (SAED) pattern was recorded to evaluate the d-spacing of lattice plane associated with YSZ nanocrystallites.

3. Results and discussion

3.1. GAXRD pattern

Figure 1 shows the annealing temperature (as-deposited, 380, 400, 450, 500, and 600 °C) dependent GAXRD pattern of YSZTFs. The presene of several sharp peaks clearly indicated the formation of highly crystalline phases of YSZ which agreed with the standard cubic structure of YSZ [29]. The observed peaks were assigned to the intense reflections from [111], [200], [220], and [311] and weak reflections from [222], [004], and [024] lattice planes associated with the nucleated nanocrystallites in the YSZTFs. Nonetheless, the diffraction pattern for all
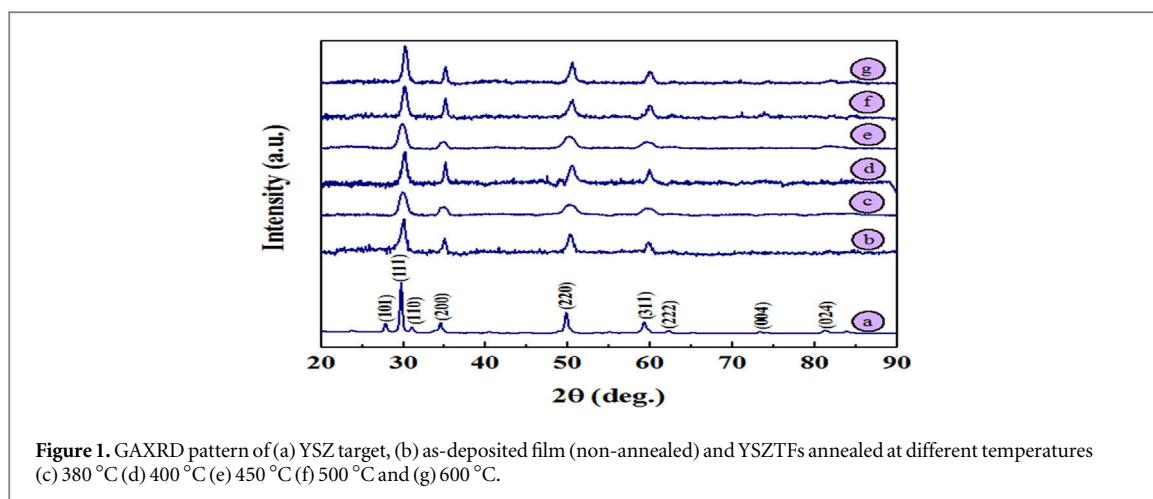
Figure 1. GAXRD pattern of (a) YSZ target, (b) as-deposited film (non-annealed) and YSZTFs annealed at different temperatures (c) 380 °C (d) 400 °C (e) 450 °C (f) 500 °C and (g) 600 °C.

Table 1. Structural properties of YSZTFs.

Annealing temperature of YSZTFs (°C)	Interplanar distance (nm)	Lattice constant (nm)	Crystallite size (nm) Scherer's formula	Crystallite size (nm) WH method	ε (%)	Crystallinity (111) (%)
As-deposited (RT)	0.2973	5.1492	13.83	10.89	0.0012	43.50
380	0.2986	5.1724	7.15	9.23	0.491	63.76
400	0.2965	5.1350	12.25	20.59	0.262	60.12
450	0.2992	5.1826	7.03	9.58	0.469	62.74
500	0.2961	5.1277	12.50	27.86	0.403	57.27
600	0.2955	5.1175	13.68	34.69	0.433	61.51

samples were nearly identical to the original YSZ target without the evidence of any other crystalline oxide phases.

Following the report of Molina-Reyes *et al* [30] or recommended JCPDS card no: 30–1468 as standard of YSZ cubic crystal the refinements of structures were performed through the lattice parameters. The grown YSZTFs were successfully refined in the cubic phase with space group Fm-3m. Depending on the full width at half maximum (FWHM, β) and the Bragg angle (θ), lattice constant (a), crystallite size (D) and lattice microstrain (ε) was calculated (table 1). Value of D was evaluated using both Scherer's formula and Williamson-Hall (WH) method [31]. The nanocrystallite sizes were increased from 9.58 nm to 34.69 nm with the increase in annealing temperature from 450 to 600 °C, respectively. As-deposited (non-annealed) sample and the one annealed at 380 °C and 400 °C showed some fluctuation in the crystallite sizes. The achieved reasonable agreements were primarily attributed to the existence of high nucleation rate assisted large microstrain in the finer grains and highly competitive grains growth mediated alteration in the crystal orientation within the film, an entropy driven mechanism. The lower order and the atomic packing density in the as-deposited YSZTFs were lower than those annealed at elevated temperatures. It was argued that annealing of films could cause reduction in the residual stress and defect in the lattice structure, leading to an increase in growth rate as reported elsewhere [32, 33].

It is worth mentioning that the occurrence of crystallization in the growth evolution temperature of YSZTF must balance the annealing process in the reaction medium. Generally, a typical setting above 400 °C leads to the formation of larger crystallite size, thereby causing diverse crystal orientations to minimize the strain energy as depicted in figure 2(a). In fact, small lattice microstrain ($\approx$0.262) and moderate crystallite size ($\approx$21 nm) reduces the defect density and porosity of the film. Present observation is consistent with the results on microstrain and crystallite size correlation effects presented by Moghaddam *et al* and Ripin *et al* [34, 35]. It was suggested that the annealing at 400 °C could possibly block the growth evolution of YSZ crystallites after sputtering. Meanwhile, the reduction of XRD intensity at 500 °C indicated a re-structuring and disordering of YSZ nanocrystalline grains. Furthermore, the improvement in the crystallinity and crystallite sizes at 600 °C was ascribed to the homogenous distribution and agglomeration of YSZ crystallites on the film surface, a similar observation made by Xu *et al* [25]. This annealing stage technique indicated that high mass diffusion inside the YSZ films seems to promote denser (columnar structures merge). Besides, it has been reported that YSZ thin film had two commonly occurring structural modifications that coexisted under annealing process which are grain growth
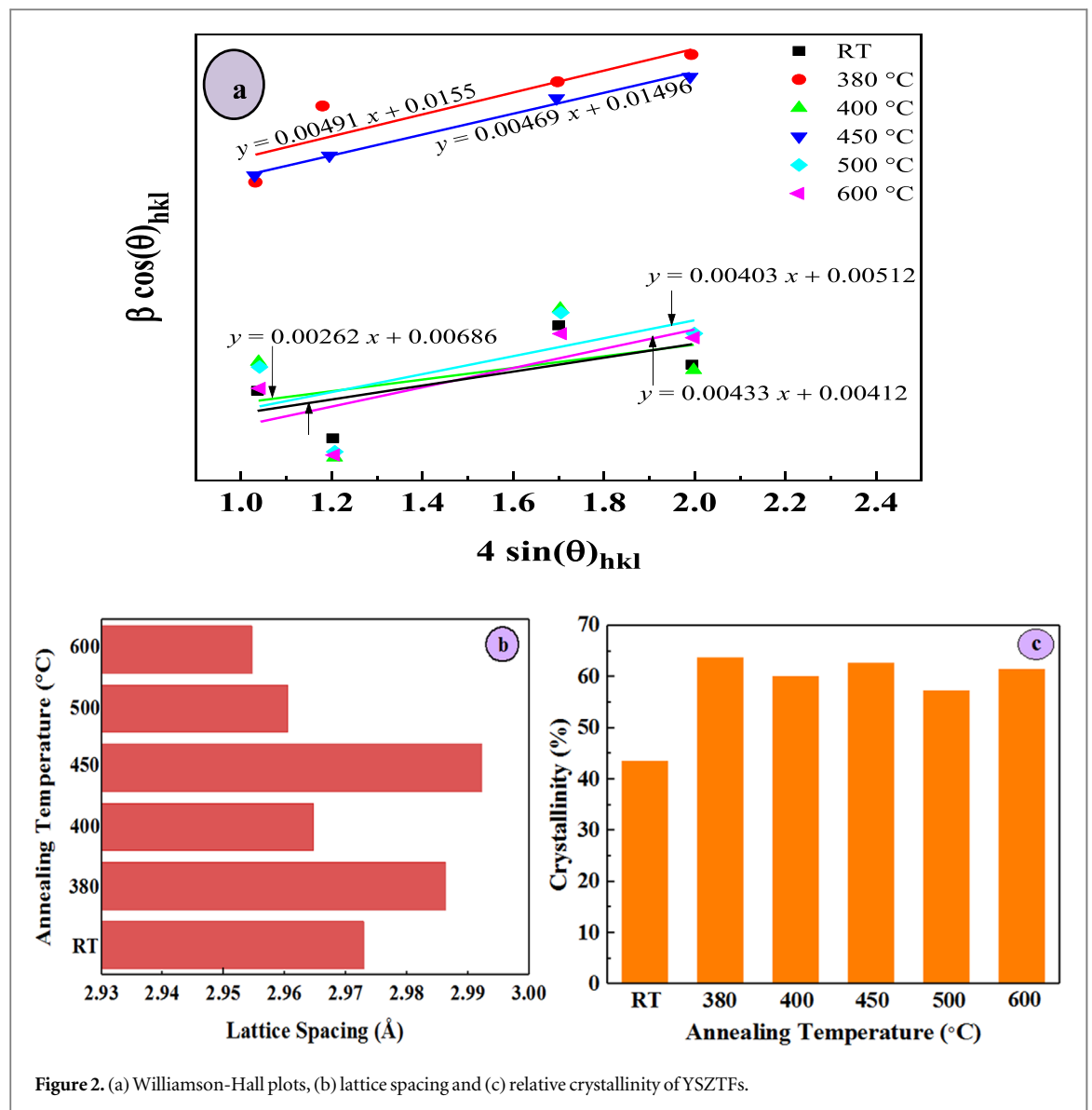
Figure 2. (a) Williamson-Hall plots, (b) lattice spacing and (c) relative crystallinity of YSZTFs.

and crystallinity. The growth of YSZ thin film was majorly attributed to two factors. First, the structure displayed an overlapping tendency during the granular growth wherein multiple crystallites could stick together. Second, these grains were stretched from one surface to another throughout the film and produced non-columnar microstructure. In short, an alteration of annealing temperature played a vital role on the grains size evolution of YSZ thin film and leads to a decrement in the film boundary area enclosing resistance to intergranular cracks suitable for low temperature-SOFCs function [36].

The position of the XRD peaks were also altered with the change in annealing temperature. Careful refinement of four intense peaks (figure 1) revealed that the value of FHWM determined using Gaussion fit were slightly higher than the one referred in the database, indicating freely distributed stress in the film [37]. Moreover, the peaks position were occurred at higher angles ($2\theta = 30.22°$, 50.51, and 59.98) for sample annealed at 600 °C compared to those synthesized at lower temperature 300 to 500 °C. This disclosure was attributed to the lattice expansion because of the presence of oxygen atoms in the YSZTFs.

Figure 2(a) illustrates the Williamson-Hall plots for all YSZTFs annealed at varied temperatures. Film annealed at 600 °C disclosed the shortest d-spacing of 0.29546 nm corresponding to (111) lattice orientations which was shortened with the increase in annealing temperature from 500 and 600 °C, whereas the crystallite size followed the opposite trend. The observed regular elongation in the d-spacing with increasing temperature (figure 2(b)) in the lower region was used as guideline to explain the effect of annealing on YSZTFs. Chopade *et al* [38] demonstrated the evidence of Y–O framework substitution into Zr–O by monitoring the regular elongting in the lattice constant (a). This revelation was attributed to the higher ionic radii of Y^{3+} compared to Zr^{3+}, wherein the substitution of Zr by Y led to the bond lengths elongation around Y and shortening around Zr atoms [33]. Generally, the preferred orientation in a polycrystalline sample produces some variations in the intensity of

selected reflection. The percent of crystallinity of YSZTFs (figure 2(c)) was expressed as the total area of crystalline peaks relative to total area of all peaks ($A_{111}/(A_{111} + A_{200} + A_{220} + A_{311})$). Relative crystallinity in the YSZTFs was determined by comparing the diffraction peaks appeared at 2θ in the range of 29.8 to 30.3 degree. Selection of this specific peak was due to least influence by the preferred crystal orientation (weak diffraction) in the film. The highest crystallinity was considered as 100% of the relative crystallinity. Film annealed at 380 °C (figure 2(c)) displayed the highest crystallinity followed by those prepared at 450 and 600 °C. The observed moderate variation in the crystallinity clearly indicated the role of annealing temperature on the growth evolution, structure and morphology of the deposited YSZTFs.

3.2. AFM images

Figures 3(a)–(f) displays the AFM images of prepared YSZTFs, which clearly revealed structural evolution in the film. The growth morphology and the surface roughness of films annealed at 380 and 400 °C were influenced significantly. Sample annealed at 450 °C showed the aggregation and agglomeration of YSZ grains, leaving behind particle cluster. However, with the increase in annealing temperature from 500 to 600 °C morphology appeared homogenous. AFM results confirmed the reconstruction of YSZ clusters and eventual nucleation and growth into condensed phase islands [22] at higher annealing temperature. Table 2 depicts the particles size, grain size and RMS surface roughness of the YSZTFs obtained from AFM micrograph analyses and Gwaddion software.

Film annealed at 500 °C and 380 °C disclosed lowest ($\approx$0.143 nm) and highest ($\approx$5.107 nm) RMS surface roughness, respectively. Particle size analysis showed a notable difference in the surface roughness pattern and grain size of YSZTFs. The lowest RMS surface roughness obtained at 500 °C implied complete homogeneous distribution of grains into fine structure which agreed with XRD analysis, suggesting annealing temperature induces preferential growth of YSZ nanocrystallites. According to Wojcieszak *et al* [39], YSZTFs with lowest RMS surface roughness ($\approx$0.14 nm) may not necessarily influence the crystallinity of the film. Film annealed at 600 °C displayed uniform and dense structure without agglomeration of moderate number of fine grains. The achieved uniformity of the film was attributed to the coalescence mechanism of YSZ particles, reducing the substrate surface area and energy. Furthermore, gap filling process between nanoparticle in the film led to the formation of completely continuous bottom-layer where grains were merged completely. Ji *et al* (2015) [40] explained that YSZTFs consisting of large grains are more likely to attain high density grain boundary, a limiting factor for ionic conduction through the lattice. Nucleation of tiny grains during crystallization have strong influence on the band gap, an effect called quantum confinement [41] which in turn can enhance the films' density, surface area, and connected nanostructure network [42]. It can be concluded that low annealing temperature significantly affects the structure and morphology of YSZTFs.

The growth process of YSZTFs can be divided into two basic steps such as deposition and crystallization. During deposition of the film, the substrate was heated wherein the crystallization required short time. In the deposition of the film, several particles needed nucleation site to build the structure by forming layers onto the substrate. Sample deposited at 300 °C revealed polycrystalline structure due to high driving force. However, crystallization of the film without annealing (as-deposited film through plasma sputtering from the target) could modify the nucleation density, surface roughness, and grain size. Sun *et al* [43] also acknowledged the filling of surface pores by ions' excited adatoms, forming a smoother surface. To verify the achieved annealing temperature mediated variation in the surface roughness and covered area in the film structure the AFM images were further analyzed using Gwyddion software where the results supported the earlier observation on crystallite size < grain size < particle size. At higher annealing temperature (500 and 600 °C), the rapid crystallization in the film was the main reason for the improved density. Consequently, continuous and regular films were formed without significant change in the morphology which suggested absence of any phase separation in the structure as agreed with the XRD data.

3.3. FESEM images

Figure 4 shows the FESEM image of all the studied YSZTFs, which revealed appreciable microstructure transformation with changing annealing temperature. As-deposited sample (without annealing) has lots of cracks and voids than the one annealed at 380 °C. Film annealed at 450 and 600 °C showed the existence of non-agglomerated fine grains without big cluster formation. Thus, the thermal effect allowed the small particles to adhere onto others to form larger grains, thereby producing sufficient crystallization confirmed by GAXRD pattern. Zheng *et al* and Lee *et al* [44, 45] reported that the nucleation process in YSZTFs at substrate temperature of 300 °C is usually characterized by columnar grains separated via dense, inter-crystalline boundaries to form more equiaxed grain structure. The growth evolution was ascribed to the diffusion of high mass adatom at $T/T_M > 0.30$; (300 °C/2600 °C). It is known that columnar structures merge easily because of thermal annealing, wherein an annealing rate $\approx$20 °C min^{-1} is advantages for test reaction to achieve denser gas
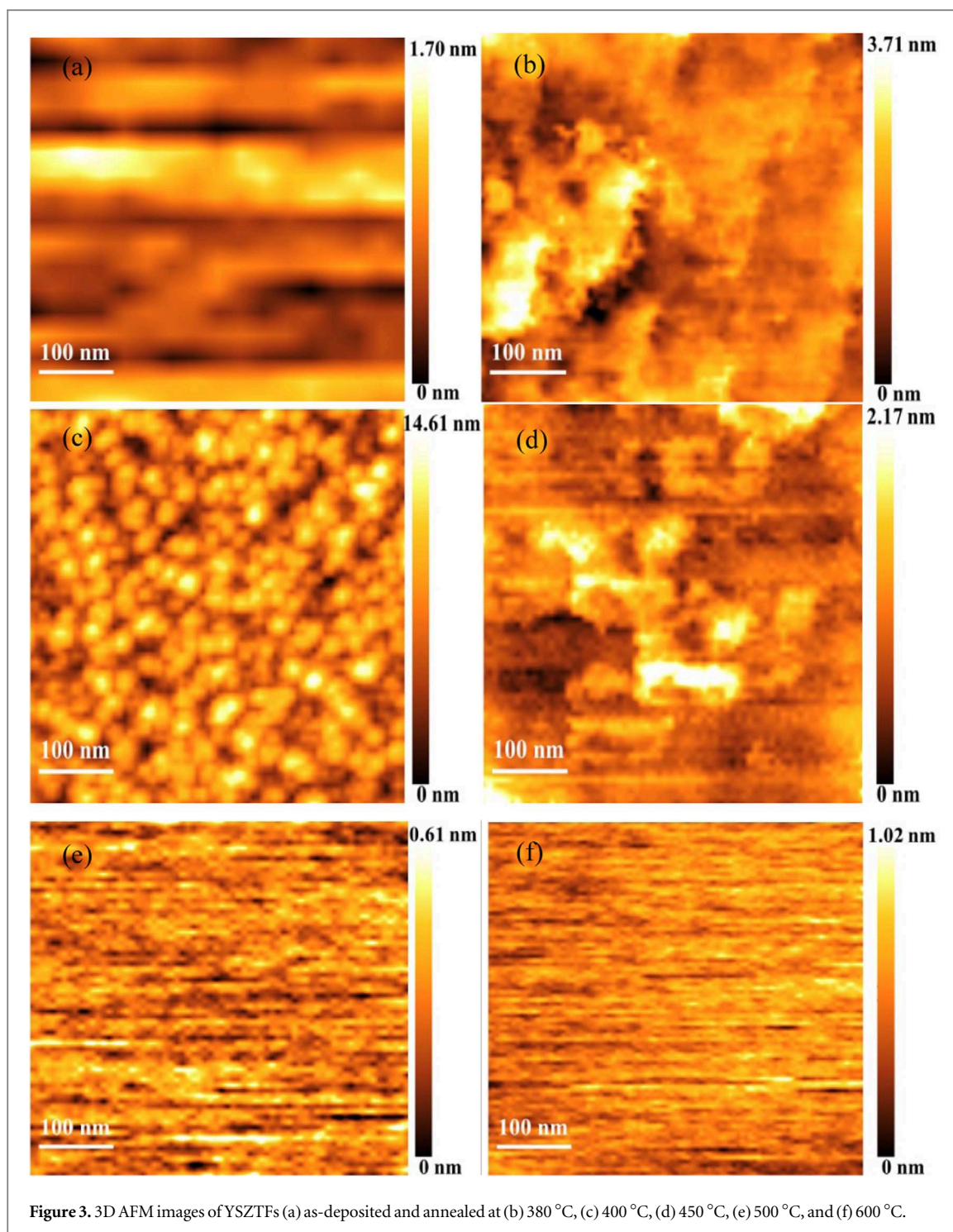
Figure 3. 3D AFM images of YSZTFs (a) as-deposited and annealed at (b) 380 °C, (c) 400 °C, (d) 450 °C, (e) 500 °C, and (f) 600 °C.

Table 2. Particles size and RMS surface roughness of the YSZTFs obtained from AFM micrograph analyses.

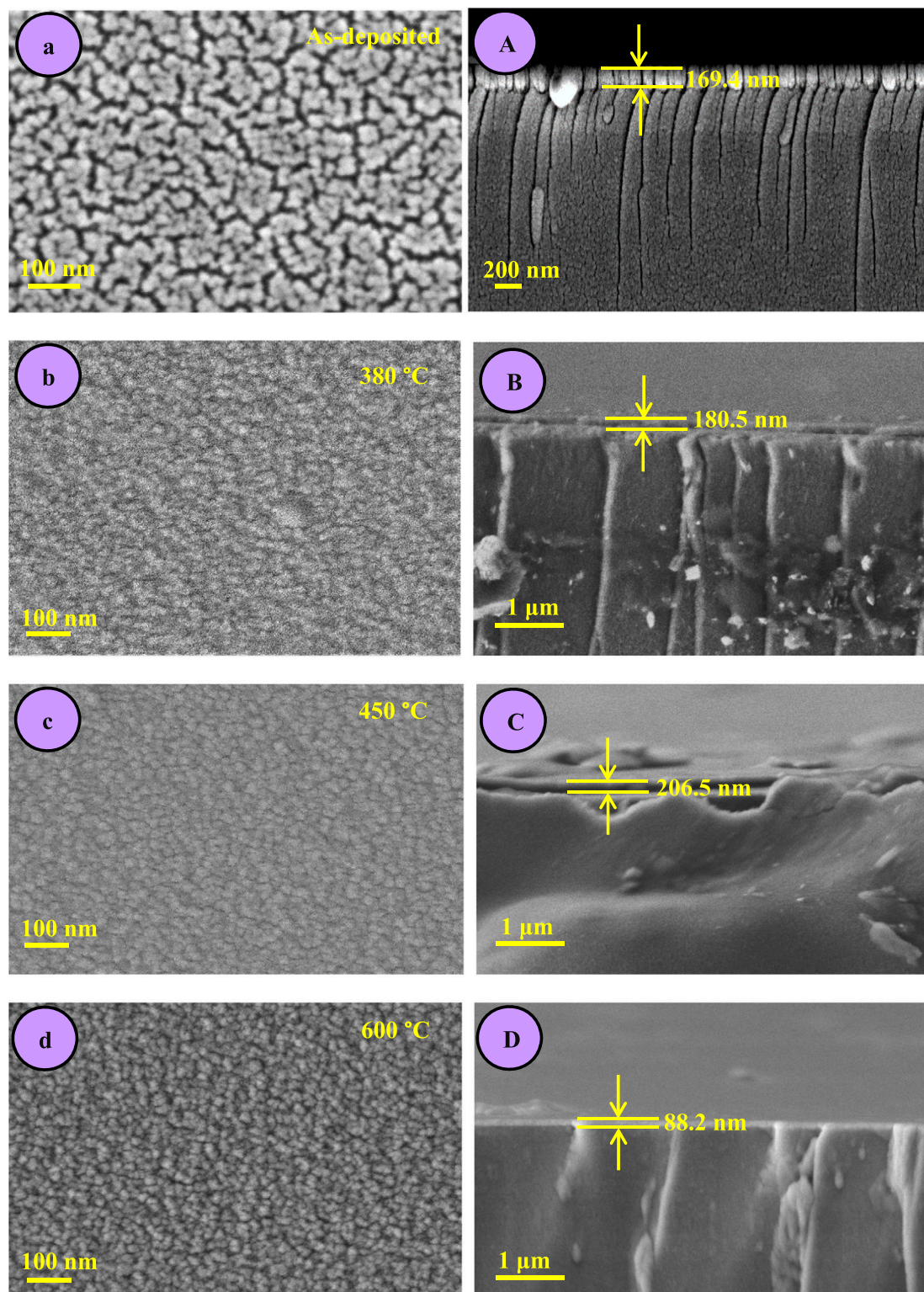| Annealing temperature of YSZTFs (°C)	Particle size using SPIWin software (nm)	RMS surface roughness (nm)
As-deposited	82.853	—
380	36.86	5.107
400	44.30	2.679
450	35.5	2.531
500	21.1	0.143
600	18.48	0.217

Figure 4. FESEM images of YSZTFs (a)–(d) Top and (A–D) cross-section view.

permeability. In brief, it was demonstrated that YSZ nanocrystallites in the film could grow to the larger sizes with the increase in annealed temperature.

The cross-section images of the film showed that its thickness was increased with the increase in annealing temperature, where non-annealed (as-deposited) film showed a lower thickness of 169.4 nm compared to the one annealed at 380 (180.5 nm) and 450 °C (206.5 nm). At higher annealing temperature (450 °C), the residual stress due to active domain dimensions and intra-granular microstrain by lattice defects played a significant role, accelerating the structural evolution through rapid crystallization process [33]. A correlation was established between d-spacing (figure 2(a) and AFM image (figure 3(d)). It was shown that larger d-spacing and clustered
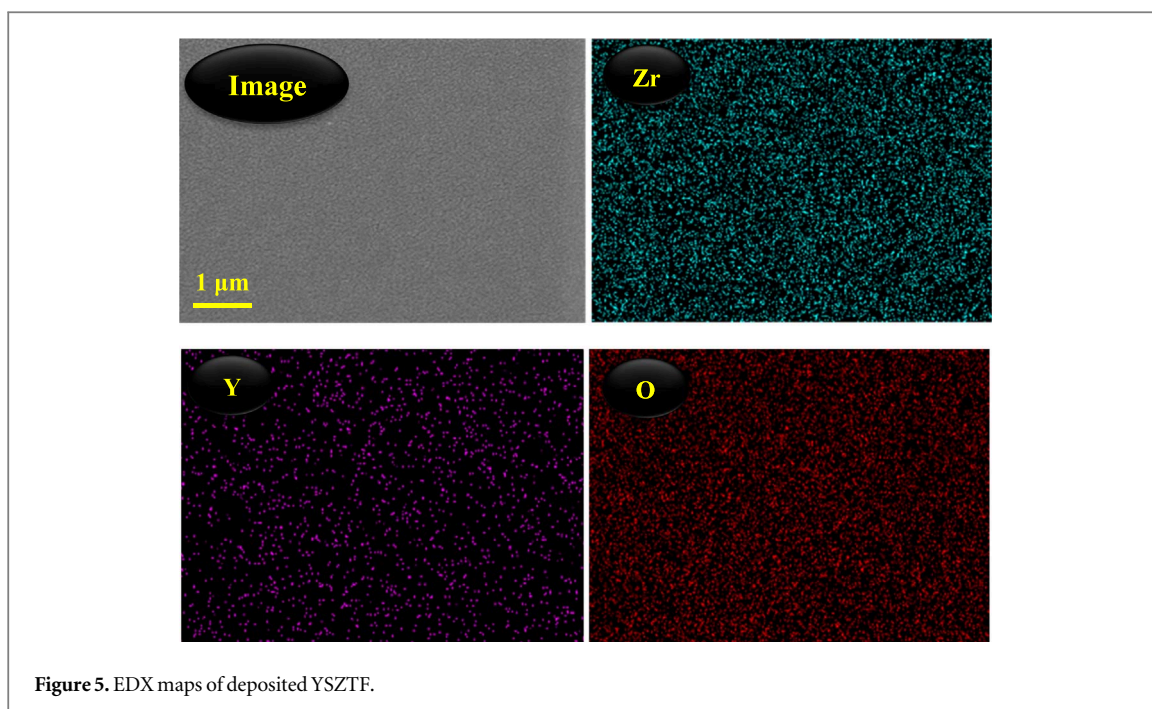
Figure 5. EDX maps of deposited YSZTF.

area could lead to the formation of non-homogenous thin film. Unlike at 600 °C, the attained lowest thickness (88.2 nm) was ascribed to the bonding strength and stacking assisted atomic growth as supported by weak intense GAXRD peaks. YSZTF annealed at 600 °C disclosed a notable difference in the homogeneity and uniformity compared to the as-deposited one. This implied the substantial transformation of particles growth with the increase in film density. This observation was consistent with the findings of Jiwoong *et al* [36]. Columnar microstructure is common because free-energetically it is easy for the grain to grow perpendicular to the substrate as narrow straight structure, indicating the beginning of copious nucleation on the substrate surface. This also suggested a competitive growth of the columnar grain during annealing at 600 °C, which in turn could enhance the overlap of grains through multiple crystallites stacking onto each other. Consequently, the single grain was stretched throughout the film surface and produce non-columnar microstructure with pinholes free films suitable for electrolyte applications.
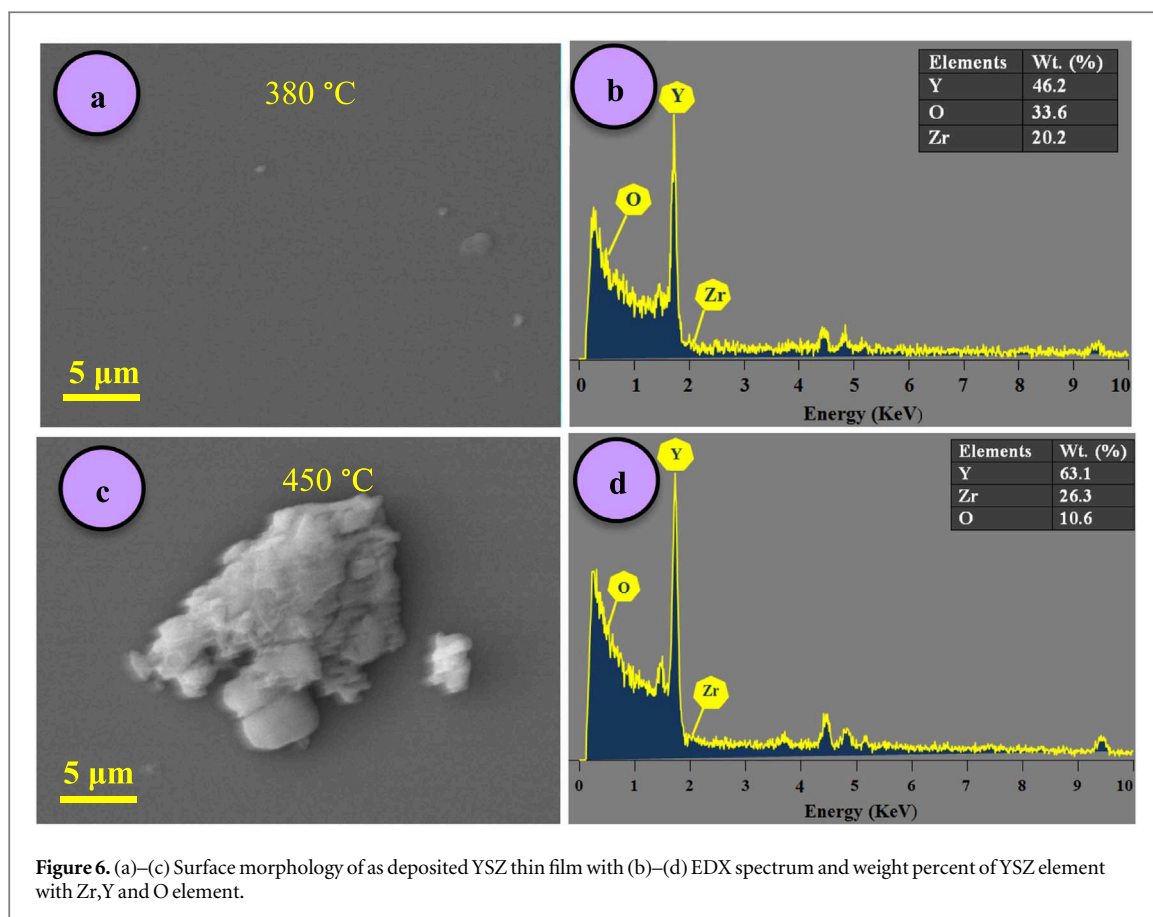
3.4. EDX spectra

Figure 5 displays the EDX map of YSZTF (as-deposited). The EDX analysis was conducted on individual crystallite of typical morphology by spot inspection with size ~1 μm. The spectra detected the chemical components of Zr (72.9 Wt%), O (17.3 Wt%) and Y(4.0%) which disclosed the uniform spread of YSZ layer on the substrate surface without any clustering, indicating the homogeneity of element distribution because of sputtering.

Figure 6 depicts the EDX spectra of two selected YSZTFs annealed at 380 and 450 °C, wherein the Zr distribution in both films were uniform with 20.21 Wt% and 26.34 Wt%, respectively. Form thermodynamic equilibrium viewpoint, Y and Zr can always form the film at temperature as low as 380 °C. However, the presence of any instability in the YSZ growth could produce gradual modification of crystal orientation and crystallinity as evidenced in figure 2. Molina-Reyes *et al* [30] applied cross-section method to detect Zr and Y diffusion and showed that with the increase in YSZ film thickness and signal for Zr and Y atom appeared stronger. Meanwhile, the reduction of O from 33.56 to 10 Wt% for film prepared corresponding to 380 and 450 °C indicated the depletion of Oxygen. The existence of high Zr^{4+} and Y^{3+} contents led to the adsorption of more atmorpheric O_2, leading to the formation of O^{2-} (oxygen loss or depletion). Thus, an exceptionally low oxygen dissolution in YSZTFs was recodred [46].

3.5. TEM images

Figure 7 presents TEM images, lattice fringe and SAED pattern of YSZTF annealed at 400 and 500 °C. By comparing the d-spacing for (111) lattice planer orientation measured from HRTEM data with the one obtained from GAXRD analysis it was estimated to be 0.30 nm. The effect of polymorph was demonstrated and the nucleation of nanocrystalline grain in the YSZTF are confirmed from the presence of Bragg contrast within the

Figure 6. (a)–(c) Surface morphology of as deposited YSZ thin film with (b)–(d) EDX spectrum and weight percent of YSZ element with Zr,Y and O element.

grains. The bright field TEM image clearly exhibited the cubic prism morphology of YSZ grain, wherein the interplanar lattice spacing for (111), (200), (220) and (311) growth orientations were determined to be 0.30, 0.27, 0.20 and 0.18 nm, respectively. Xu *et al* [25] have also reported similar findings for YSZ film.

The high-resolution TEM image of selected region disclosed the characteristic crystal structure of YSZTF preapred 400 °C, revealing uniform grains without any dislocation networks in the structure. Meanwhile, an increase in the annealing temperature to 500 °C produce few dislocation network (dash line) in the film. Thus, the observed slight difference in the crystallinity for the two sample prepared at 400 and 500 °C was attributed to the presence of residual stress effect and oxygen vacancies that could be disorderedly distributed among the coating as acknowledged by Yeh *et al* and Shi *et al* [47–49]. YSZTF annealed at 500 °C was thinner than the one prepared with 400 °C. Similar observation was made by Takayanagi *et al* [50] where a correlation between the contraction of the cell in Y–O and Zr–O TFs was established. Thinner film with smaller particles and grains were also observed because more SiO_2/YSZ interface was distorted into the lattice. The oxygen vacancies mediated high alteration in the structure and morphology at the YSZ grain surface was majorly responsible for producing smaller d-spacing.

4. Conclusions

The highly crystalline and dense YSZTFs were deposited by RF magnetron sputtering technique. It was shown that by adjusting the annealing temperature the structure and morphology of grown films can be customized. The achieved YSZTFs displayed ionic character due to the occurrences of Y–O and Zr–O functional group in the materials' framework. Films annealed from 380 to 400 °C revealed a crystallinity of 67% and amorphosity of 33%, dense and homogenous microstructure with moderate particle size without any dislocation in the lattice network. These excellent features of the deposited YSZTFs were primarily ascribed to complex growth mechanisms aroused from the grain size differences at nanoscale. Prolong annealing of the film was found to destroy the crystallinity, thereby made the film more thin. It is worth to examine the effects of annealing temperature on the overall conductivity and the activation energy of the YSZTFs.
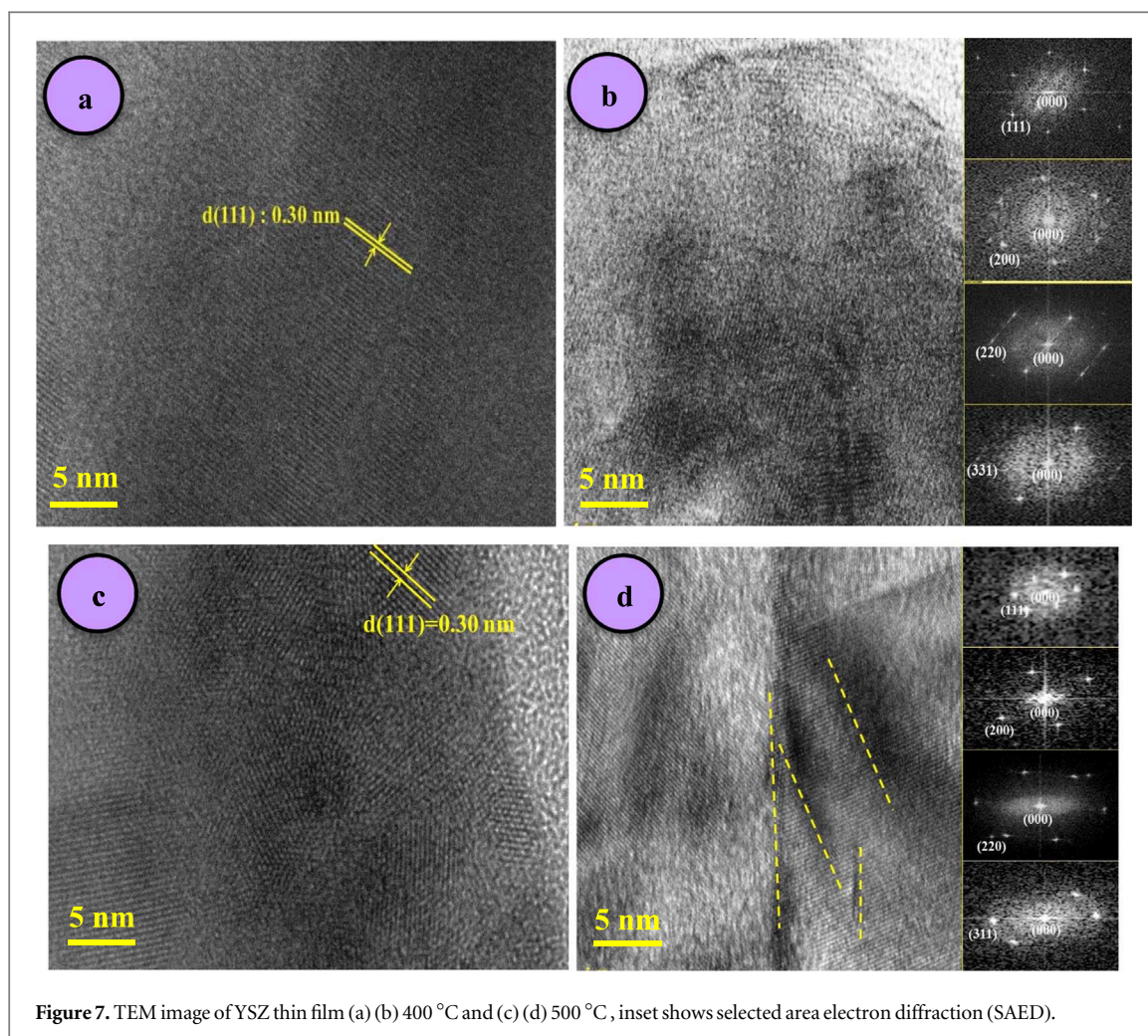
Figure 7. TEM image of YSZ thin film (a) (b) 400 °C and (c) (d) 500 °C, inset shows selected area electron diffraction (SAED).

Acknowledgments

ORCID iDs

N A Rusli https://orcid.org/0000-0002-6114-621X
N Nayan https://orcid.org/0000-0002-9962-5283

References

[1] Halimah S, Munira S, Hafiz M, Othman D and Rahman M A 2016 Co-extruded dual-layer hollow fiber with different electrolyte structure for a high temperature micro-tubular solid oxide fuel cell *Int. J. Hydrogen Energy* **42** 9116–24
[2] Kuhn M and Napporn T W 2010 Single-Chamber solid oxide fuel cell technology-from its origins to today's state of the art *Energies.* **3** 57–134
[3] Sahli Y, Ben H and Zitouni B 2018 Optimization study of the produced electric power by SOFCs *Int. J. Hydrogen Energy* **44** 1–10
[4] Fleischhauer F, Tiefenauer A, Graule T, Danzer R, Mai A and Kuebler J 2014 Failure analysis of electrolyte-supported solid oxide fuel cells *J Power Sources* **258** 382–90
[5] Roehrens D, Packbier U, Fang Q, Blum L, Sebold D, Bram M and Menzler N 2016 Operation of Thin-film electrolyte metal-supported solid oxide fuel cells in lightweight and stationary stacks: material and microstructural aspects *Materials (Basel)* **9** 762
[6] Saebea D, Authayanun S and Patcharavorachot Y 2017 Electrochemical performance assessment of low- temperature solid oxide fuel cell with YSZ-based and SDC-based electrolytes *Int. J. Hydrogen Energy* **43** 921–31
[7] Asadikiya M, Sabarou H, Chen M and Zhong Y 2016 Phase diagram for a nano-yttria-stabilized zirconia *RSC Adv.* **6** 17438–45
[8] Frison R, Heiroth S, Rupp J L M, Conder K, Barthazy E J, Müller E, Horisberger M, Döbeli M and Gauckler L J 2013 Crystallization of 8 mol % yttria-stabilized zirconia thin- films deposited by RF-sputtering *Solid State Ionics* **232** 29–36
[9] Dubbink D, Koster G and Rijnders G 2018 Growth mechanism of epitaxial YSZ on Si by Pulsed Laser Deposition *Sci. Rep.* **8** 2–11

[10] Zambrano D F, Barrios A, Tobón L E, Serna C, Gómez P, Osorio J D and Toro A 2018 Thermal properties and phase stability of Yttria-Stabilized Zirconia (YSZ) coating deposited by air plasma spray onto a Ni-base superalloy *Ceram. Int.* **44** 3625–35

[11] Viazzi C, Bonino J P, Ansart F and Barnabé A 2008 Structural study of metastable tetragonal YSZ powders produced via a sol-gel route *J. Alloys Compd.* **452** 377–83

[12] Doleker K M, Ahlatci H and Karaoglanli A C 2017 Investigation of isothermal oxidation behavior of thermal barrier coatings (TBCs) consisting of YSZ and multilayered YSZ/Gd$_2$Zr$_2$O$_7$ ceramic layers *Oxid. Met.* **88** 109–19

[13] Sun C, Li H and Chen L 2012 Nanostructured ceria-based materials: synthesis, properties, and applications *Energy Environ. Sci.* **5** 8475–505

[14] Tanveer W H, Ji S, Yu W, Cho G Y, Lee Y H and Cha S W 2015 Intermediate-temperature solid-oxide fuel cells with a gadolinium-doped ceria anodic functional layer deposited via radio-frequency sputtering *J Nanosci Nanotechno* **15** 8926–30

[15] Schlupp M V F, Prestat M, Martynczuk J, Rupp J L M, Bieberle-Hütter A and Gauckler L J 2012 Thin film growth of yttria stabilized zirconia by aerosol assisted chemical vapor deposition *J. Power Sources* **202** 47–55

[16] Chen L and Yang G J 2017 Anomalous epitaxial growth in thermally sprayed YSZ and LZ splats *J. Therm. Spray Technol.* **26** 1168–82

[17] Akasaka S 2016 Thin film YSZ-based limiting current-type oxygen and humidity sensor on thermally oxidized silicon substrates *Sensors Actuators, B Chem.* **236** 499–505

[18] Chroneos A, Yildiz B, Tarancón A, Parfitt D and Kilner J A 2011 Oxygen diffusion in solid oxide fuel cell cathode and electrolyte materials: mechanistic insights from atomistic simulations *Energy Environ. Sci.* **4** 2774–89

[19] Cadi-essadek A, Roldan A and De Leeuw N H 2016 Surface Science Density functional theory study of the interaction of H$_2$O, CO$_2$ and CO with the ZrO$_2$ (111), Ni/ZrO$_2$ (111), YSZ (111) and Ni/YSZ (111) *Surfaces* **653** 153–62

[20] Sochugov N S, Soloviev A A, Shipilova A V, Rabotkin S V, Rotshtein V P and Sigfusson I T 2013 The effect of pulsed electron beam pretreatment of magnetron sputtered ZrO$_2$:Y$_2$O$_3$ films on the performance of IT-SOFC *Solid State Ionics* **231** 11–7

[21] Yao L, Ou G, Nishijima H and Pan W 2015 Enhanced conductivity of (110)-textured ScSZ films tuned by an amorphous alumina interlayer *Phys. Chem. Chem. Phys.* **17** 23034–40

[22] Tanhaei M and Mozammel M 2017 Yttria-stabilized zirconia thin film electrolyte deposited by EB-PVD on porous anode support for SOFC applications *Ceram. Int.* **43** 3035–42

[23] Co-sputtering R F P D, Hwang S, Lee J H, Kim Y Y, Yun M G, Lee K, Lee J Y and Cho H K 2014 Microstructural Characteristics of Tin Oxide-Based Thin *J Nanosci Nanotechnol* **14** 8908–14

[24] Meškinis Š, Čiegis A, Vasiliauskas A, Člapikas K, Tamulevičius T, Andrulevičius M, Niaura G and Tamulevičius S 2016 Effects of the high power pulsed magnetron sputtering deposition conditions on structure of diamond like carbon:Cu films *J. Nanosci. Nanotechnol.* **16** 10133–42

[25] Xu Y-B, Kang Z-F, Fan Y, Xiao L-L, Bo Q-R and Ding T-Z 2016 Electrical properties of the YSZ/STO/YSZ-STO superlattice electrolyte film at low temperatures *Russ. J. Phys. Chem. A* **90** 485–90

[26] Bernard B and Schick V 2017 Effect of Suspension Plasma-Sprayed YSZ Columnar Microstructure and Bond Coat Surface Preparation on Thermal Barrier Coating Properties *J Therm Spray Techn* **26** 1025–37

[27] Markocsan N, Nyle P, Ganvir A, Curry N, Bjo S, Markocsan N, Nyle P and Science E 2015 Characterization of Microstructure and Thermal Properties of YSZ Coatings Obtained by Axial Suspension Plasma Spraying (ASPS) *J Therm Spray Techn* **24** 1195–204

[28] Hill T, Huang H, Hill T and Huang H 2011 Fabricating pinhole-free YSZ sub-microthin films by magnetron sputtering for micro-SOFCs *Int. J. Electrochem.* **2011** 1–8

[29] Coddet P, Caillard A, Vulliet J, Richard C and Thomann A L 2018 Multistep magnetron sputtering process and *in situ* heat treatment to manufacture thick, fully oxidized and well crystallized YSZ films *Surf. Coatings Technol.* **349** 133–43

[30] Molina-Reyes J, Tiznado H, Soto G, Vargas-Bautista M, Dominguez D, Murillo E, Sweeney D and Read J 2018 Physical and electrical characterization of yttrium-stabilized zirconia (YSZ) thin films deposited by sputtering and atomic-layer deposition *J. Mater. Sci., Mater. Electron.* **29** 1–9

[31] Salari S and Ghodsi F E 2017 A significant enhancement in the photoluminescence emission of the Mg doped ZrO$_2$ thin films by tailoring the effect of oxygen vacancy *J. Lumin.* **182** 289–99

[32] Xiufeng T 2017 Effects of the annealing heating rate on sputtered aluminum oxide films *J. Wuhan Univ. Technol. Sci.* **32** 94–9

[33] Heiroth S, Frison R, Rupp J L M, Lippert T, Barthazy E J, Müller E, Döbeli M, Conder K, Wokaun A and Gauckler L J 2011 Crystallization and grain growth characteristics of yttria-stabilized zirconia thin films grown by pulsed laser deposition *Solid State Ionics* **191** 12–23

[34] Moghaddam H M and Nasirian S 2012 Dependence of activation energy and lattice strain on TiO$_2$ nanoparticles *J. Exp. Nanoscience.* **1** 201–12

[35] Ripin A, Mohamed F, Choo T F, Yusof M R, Hashim S and Ghoshal S K 2018 X-ray shielding behaviour of kaolin derived mullite-barites ceramic *Radiat. Phys. Chem.* **144** 63–8

[36] Bae J, Chang I, Kang S, Hong S, Cha S W and Kim Y B 2014 Post-annealing of thin-film yttria stabilized zirconia solid oxide fuel cells *J. Nanosci. Nanoechnology.* **14** 9294–9

[37] Sønderby S, Christensen B H and Almtoft K P 2014 Magnetron sputtered Gadolina-doped Ceria Diffusion Barriers for Metal-supported Solid Oxide Fuel Cells *J Power Sources* **267** 452–8

[38] Chopade S S *et al* 2015 RF plasma enhanced MOCVD of yttria stabilized zirconia thin films using octanedionate precursors and their characterization *Appl. Surf. Sci.* **355** 82–92

[39] Wojcieszak D, Kaczmarek D and Mazur M 2012 Photocatalytic properties of transparent TiO$_2$ coatings doped with neo- dymium *J. Chem. Technol.* **14** 1–7

[40] Ji S, Cho G Y, Yu W, Su P, Lee M H and Cha S W 2015 Plasma-enhanced atomic layer deposition of nanoscale yttria- stabilized zirconia electrolyte for solid oxide fuel cells with porous substrate *Appl. Mater. Interfaces.* **7** 2998–3002

[41] Henkel B, Neubert T, Zabel S, Lamprecht C, Selhuber-Unkel C, Rätzke K, Strunskus T, Vergöhl M and Faupel F 2016 Photocatalytic properties of titania thin films prepared by sputtering versus evaporation and aging of induced oxygen vacancy defects *Appl. Catal. B Environ.* **180** 362–71

[42] Quan X, Sun B and Xu H 2015 Anode decoration with biogenic Pd nanoparticles improved power generation in microbial fuel cells *Electrochim. Acta* **182** 815–20

[43] Sun H, Ma W, Yu J, Chen X, Sen W and Zhou Y 2012 Preparation and characterization of La$_{0.9}$Sr$_{0.1}$Ga$_{0.8}$Mg$_{0.2}$O$_{3-\delta}$ thin film electrolyte deposited by RF magnetron sputtering on the porous anode support for IT-SOFC *Vacuum* **86** 1203–9

[44] Zheng Z, Luo J and Li Q 2015 Mechanism of competitive grain growth in 8YSZ splats deposited by plasma spraying *J. Therm. Spray Technol.* **24** 885–91

[45] Lee Y H, Chang I, Cho G Y, Park J, Yu W and Tanveer W H 2018 Thin film solid oxide fuel cells operating below 600 °C: a review *Int. J. Precis. Eng. Manuf.—Green Technol.* **5** 441–2

[46] Duan Y, Zhang M, Wang L, Wang F, Yang L, Li X and Wang C 2017 Plasmonic Ag-TiO$_2$ − xnanocomposites for the photocatalytic removal of NO under visible light with high selectivity: the role of oxygen vacancies *Appl. Catal. B Environ.* **204** 67–77

[47] Yeh T H, De Lin R and Cherng J S 2013 Significantly enhanced ionic conductivity of yttria-stabilized zirconia polycrystalline nano-film by thermal annealing *Thin Solid Films* **544** 148–51

[48] Shi Z, Shum P, Zhou Z and Li L K Y 2017 Effect of oxygen flow ratio on the wetting behavior, microstructure and mechanical properties of CeO$_2$−xcoatings prepared by magnetron sputtering *Surf. Coatings Technol.* **320** 333–8

[49] Li Y, Wang S and Su P 2016 Proton-conducting micro-solid oxide fuel cells with improved cathode reactions by a nanoscale thin film gadolinium-doped ceria interlayer *Sci. Educ.* **6** 1–9

[50] Takayanagi M, Tsuchiya T, Kawamura K, Minohara M, Horiba K, Kumigashira H and Higuchi T 2017 Thickness-dependent surface proton conduction in (111) oriented yttria-stabilized zirconia thin film *Solid State Ionics* **311** 46–51